Journal of Alloys and Compounds 511 (2012) 22–30

Contents lists available at SciVerse ScienceDirect

Journal of Alloys and Compounds

journal homepage: www.elsevier.com/locate/jallcom

Grain size dependent magnetization, electrical resistivity and magnetoresistance in mechanically milled $La_{0.67}Sr_{0.33}MnO_3$

I. Panneer Muthuselvam, R.N. Bhowmik*

Department of Physics, Pondicherry University, R. Venkataraman Nagar, Kalapet, Pondicherry 605014, India

ARTICLE INFO

Article history:
Received 28 July 2011
Received in revised form
14 September 2011
Accepted 15 September 2011
Available online 21 September 2011

Keywords:
Ferromagnetic manganite
Magnetic grain size effects
Magnetic freezing
Low temperature magnetic anomaly
High field magnetoresistance

ABSTRACT

We have studied magnetization, ac susceptibility, resistivity and magnetoresistance in mechanically milled $La_{0.67}Sr_{0.33}MnO_3$. The material with grain size micron to nanometer scale has stabilized in rhombohedral crystal structure with space group *R*3*C*. We have found various grain size effects, e.g., decrease of ferromagnetic moment, increase of surface spin disorder, and appearance of insulator/semiconductor type resistivity. In addition to these conventional features, we have identified a magnetic anomaly at 45 K in bulk sample. Ferromagnetic to paramagnetic transition temperature (T_C) is above room temperature for all samples. The samples are typical soft ferromagnet that transformed from multi-domain state to single domain state in nanocrystalline samples. The remarkable observation is that low temperature freezing of ferromagnetic domains/clusters does not follow the conventional spin glass features. Experimental results clearly showed the enhancement of high field magnetoresistance in nanocrystalline samples below 200 K, whereas low field magnetoresistance gradually decreases above 200 K and almost absent at 300 K. We have discussed few more magnetic and electrical changes, highly relevant to the progress of nanomaterial research in ferromagnetic manganites.

1. Introduction

Ferromagnetic manganites ($La_{1-x}A_xMnO_3$; A: Sr, Ba, Ca) have opened a wide scope of technological applications in magnetic recording, sensors, magneto-electronics devices [1–3]. Most of the recent works on ferromagnetic manganites are driving towards the realization of low temperature magnetic (frustration in ferromagnetic ground state) and electric (resistivity minimum, metallic to insulator/semiconductor feature, low field magnetoresistance (LFMR)) properties of nano-grained particles [3–5]. Among the ferromagnetic manganites, $La_{0.67}Sr_{0.33}MnO_3$ (LSMO) is attractive because of its large magnetic moment, high value of ferromagnetic to paramagnetic transition temperature $T_C \sim 370$ K, and large LFMR [6–10]. Various mechanisms, e.g., ferromagnetic double exchange interactions between $Mn^{3+}(d^4)(t_{2g}{}^3e_g{}^1, s = 2)$ and $Mn^4(d^3)(t_{2g}{}^3e_g{}^0, s = 3/2)$ ions [11], electron–phonon coupling [12], magnetic clustering and phase separation in ferromagnetic matrix [13], and grain boundary spin disorder [14], have been proposed to explain many magnetic and electrical properties in manganites.

There is some low temperature magnetic anomaly in manganite nanoparticles, which was attributed to surface spin freezing effect of nano-sized grains. For example, Dey et al. [15] in $La_{0.7}Ca_{0.3}MnO_3$ nanoparticles and Zhu et al. [9] in $La_{0.67}Sr_{0.33}MnO_3$ nanoparticles observed such magnetic anomaly at about 40–45 K mainly in field cooled magnetization (MFC) curve. Zhu et al. [9] showed that the low temperature anomaly become less pronounced as the grain size increases in $La_{0.67}Sr_{0.33}MnO_3$. Unfortunately, there is no comparison between anomalous MFC features of nanoparticles and their bulk counterpart. Markovich et al. [16] observed an unusual magnetic glassy phase in $La_{0.8}Ca_{0.2}MnO_3$ nanoparticles. Average particle size of 18 nm has shown superspin-glass and superferromagnetic features, associated with memory effects in zero-field-cooled (ZFC) and field-cooled (FC) magnetization. The ensembles of 70 nm particles showed minor irreversibility between ZFC and FC magnetization and no frequency dependent ac susceptibility. These features are different from spin glass like feature in $La_{0.7}Ca_{0.3}MnO_3$ nanoparticle [17]. Although clustering has a strong effect on the nature of magnetic ground state in manganite particles [3,18], the work by Wang et al. [19] suggested antiferromagnetic phase disappearance and better stabilization of ferromagnetic phase in $Ca_{0.82}La_{0.18}MnO_3$ nanoparticles. Another puzzling observation is the low temperature resistivity minimum in manganites [20–23]. Various proposals came forward to explain this feature [15,20,21]. For example, tunneling of electronic charge carriers between ferromagnetic grains through grain boundaries is well-accepted mechanism. The counter argument [24–26] is that additional scattering from spin disordered grain boundaries is responsible for low temperature resistivity up turn. Many reports on manganites [15,27,28] showed that the low temperature

* Corresponding author. Tel.: +91 9944064547; fax: +91 4132655734.
E-mail address: rnbhowmik.phy@pondiuni.edu.in (R.N. Bhowmik).

0925-8388/$ – see front matter © 2011 Elsevier B.V. All rights reserved.
doi:10.1016/j.jallcom.2011.09.046

resistivity is maximum for grain size down to nanometer scale, although it is not the universal feature for all manganite nanoparticles. In contrast, Kundu et al. [29] reported the suppression of ferromagnetic insulating state and stabilization of metallic state when grain size of $Nd_{0.8}Sr_{0.2}MnO_3$ decreases down to 42 nm.

Hence, certain aspects of the magnetism (spontaneous magnetization, coercivity, spin glass and superparamagnetic blocking) and electrical properties (magnetoresistance, resistivity minimum at low temperature) of manganite particles need proper address in the light of surface spin disorder, magnetic heterogeneity and core–shell structure of ferromagnetic particles [4,8,30]. Although most of the reports focused on chemical routed samples, we believe mechanically milled manganites could be more effective for tailoring surface/grain boundary spin disorder. In addition to the contribution of surface spin disorder and magnetic inhomogeneity [31], micro-strain induced properties can be studied in mechanically milled samples [32–34]. Motivated by the interesting magnetic modifications in mechanically milled $La_{0.67}Sr_{0.33}MnO_3$ nanoparticles [31,35], we wish to examine the low temperature magnetism and magneto-resistance of mechanically milled $La_{0.67}Sr_{0.33}MnO_3$ nanoparticles assuming highly spin ordered ferromagnetic core as metallic, and spin disordered shell as electrically insulator/semiconductor.

2. Experimental

Nanocrystalline $La_{0.67}Sr_{0.33}MnO_3$ samples were prepared by mechanically milling of bulk material. The bulk sample was prepared by solid state sintering of high purity La_2O_3 (99.9%), $SrCO_3$ (99.9%) and MnO_2 (99.99%) powders. Stoichiometric amount of the powders was ground for 2 h to obtain better homogeneous mixture before firing at 600 °C for 5 h to remove CO_2. The mixture was finally sintered at 1300 °C for 40 h in air with intermediate cooling to room temperature and subsequent grinding. The heating and cooling rate was maintained nearly 5 °C/min. Fritsch Planetary Mono Miller (P6) was used for milling of powdered bulk material in a 45 ml agate bowl. Non-magnetic silicon nitride and tungsten carbide balls were mixed in powdered material and milling was performed in air. Small amount of milled powder was taken out from the bowl after 25 h, 80 h, 160 h and 300 h milling to check the formation of nanostructured material. Samples were denoted as MH0, MH25, MH80, MH160 and MH300 for milling time 0 (bulk), 25, 80, 160 and 300 h, respectively. In order to study the thermal annealing effects MH300 sample was annealed at 600 °C for 6 h. This heat-treated sample was denoted as MH300A6.

Crystalline structure of the samples was identified using room temperature X-ray diffraction (XRD) spectrum by employing X-Pert PANalytical diffractometer. XRD spectrum was recorded using Cu Kα radiation in the 2θ range 10–90° with step size 0.01°. Surface morphology was studied using scanning electron microscope (SEM) image (HITACHI S-3400N, Japan). Elemental analysis of the samples was carried out using Energy Dispersive analysis of X-ray (EDX) spectrometer (Thermo electron corporation Instrument, USA). Temperature (5–300 K) and magnetic field (0 to ±50 kOe) dependent dc magnetization was measured using MPMS (Quantum Design, USA). AC susceptibility was studied using home made ac susceptometer [36]. Magnetoresistance of the samples was measured using PPMS (Quantum Design, USA). The dc resistivity and magneto-resistance of the bar shaped samples were measured by four-probe method. Fine electrical contacts were made using copper wire, and silver paste was used to make the point contacts. The current was allowed to pass through two outer point contacts whereas voltage was measured between inner point contacts.

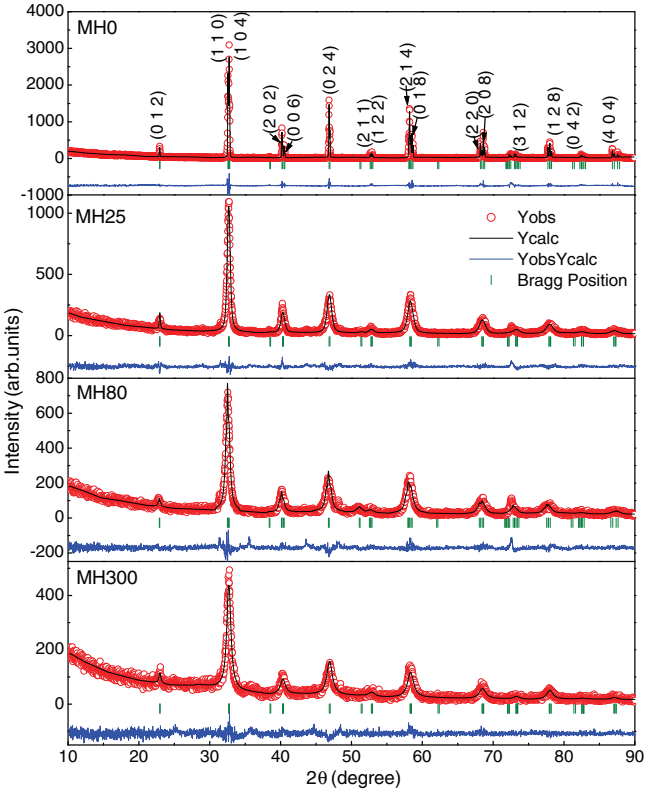

Fig. 1. Room temperature XRD pattern (red symbol) and Rietveld profile file (black like) of MH0, MH25, MH80 and MH300 samples. (For interpretation of the references to color in this figure legend, the reader is referred to the web version of the article.)

3. Results and discussion

3.1. Structure and surface morphology

Fig. 1 shows XRD profiles of bulk, milled and thermal heated MH300A6 samples. The profiles were fitted using FULLPROF-Suite program. XRD pattern of the samples matched into rhombohedral structure with space group *R*3*C*. There was no trace of significant impurity phase in the samples. Lattice parameters of bulk sample are in good agreement with reported values ($a = b = 5.492(5)$ Å, $c = 13.365(9)$ Å [3]). Fig. 2(a) shows the decrease of "*a*" with the increase of milling time. However, lattice parameter "*c*" (Fig. 2(a)) and cell volume "*V*" (Fig. 2(b)) both have initially increased with milling time up to 80 h (MH80 sample) and thereafter, decreased on increasing milling time. EDX spectra (example given for MH80 sample in Fig. 2(c)) have identified La, Sr, Mn and O as the constituent elements in bulk and milled samples. The average atomic ratio of the elements La:Sr:Mn was found as 0.66:0.33:1, 0.65:0.31:1,

Table 1
Grain size and strain from XRD spectra, particle size from SEM. Different magnetic parameters: saturation magnetization (M_{Sat}), spontaneous magnetization (M_S), M_r/M_S at 10 K and 300 K, and coercivity (H_C) at 10 K.

Sample	Grain size (nm)	Strain (ε)	Particle size (nm)	M_{Sat} (μ_B/f.u.)		M_S (μ_B/f.u.)		M_r/M_S 10 K	H_C (Oe) 10 K
				10 K	300 K	10 K	300 K		
MH0	–	–	~3000	3.49	2.54	3.47	2.35	0.15	50
MH25	16	0.43	85	2.51	1.53	2.36	1.19	0.26	88
MH80	12	0.48	82	1.84	0.94	1.56	0.68	0.31	337
MH160	11	0.52	80	1.24	0.61	1.02	0.40	0.37	407
MH300	9	0.56	72	1.17	0.59	0.93	0.38	0.31	664
MH300A6	14	0.41	86	1.44	0.77	1.26	0.53	0.36	319

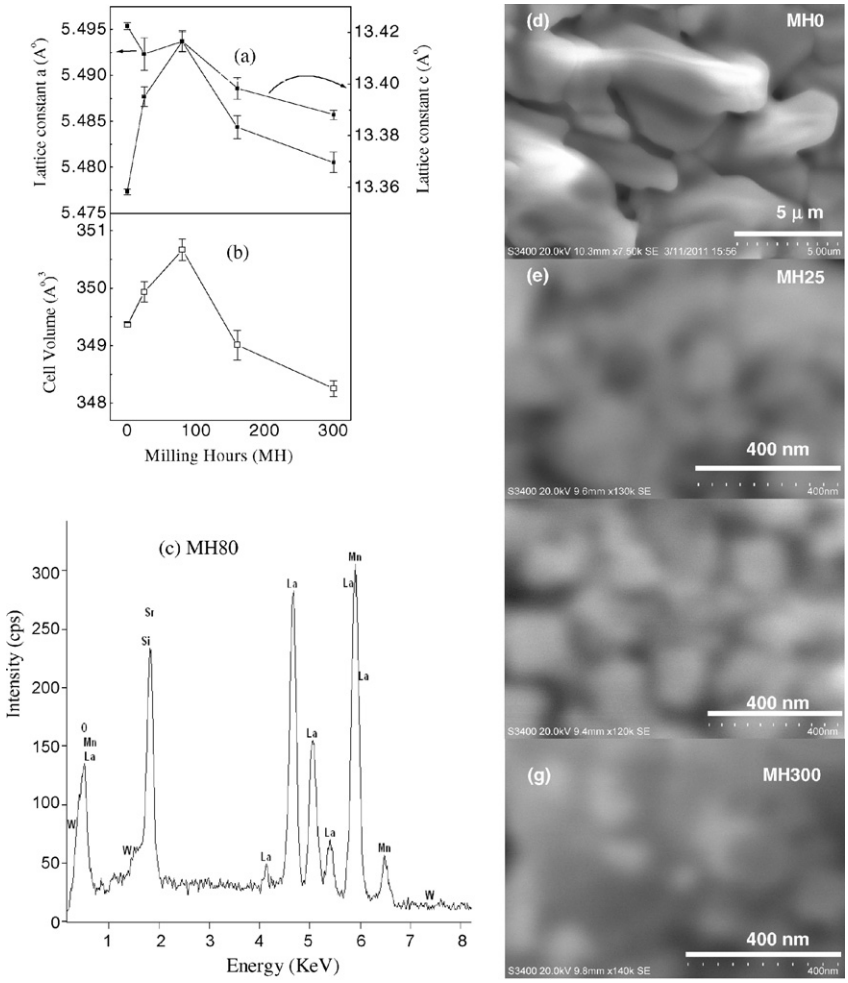

Fig. 2. (a) Lattice parameters a (left), c (right) and cell volume (b) varies with function of milling hours samples of LSMO. (c) EDAX spectra of MH80 sample. (d–g) SEM picture of MH0, MH25, MH80 and MH300 samples, respectively.

0.66:0.31:1, 0.65:0.32:1 and 0.65:0.31:1 for MH0, MH25, MH80, MH160 and MH300 samples, respectively. The oxygen content of the samples is in the range 2.95–3 per formula unit. This elemental composition is close to the expected value of La:Sr:Mn (0.67:0.33:1). EDX spectra also identified minor traces of Si (<1 at.%) and W (<0.2 at.%) in the samples with milling time 160 h and 300 h. These non-magnetic contaminants increase disorder at the grain boundaries and we do not expect their significant impact on the magnetic properties of the milled samples. Grain (crystallite) size and micro strain (ε) of the milled samples were calculated using Williamson–Hall method [37]. The results in Table 1 confirmed the decrease of grain size with substantial increase of micro-strain with milling time. Thermal activated grain growth kinetics and better crystallization at the grain boundaries of nanocrystalline structure once again increased the grain size and reduced micro-strain in MH300A6 sample. SEM images in Fig. 2(d–g) indicated the reduction of micron-sized particles of bulk sample into nearly spherical shaped nano-sized particles in milled samples. Table 1 shows that SEM value is large in comparison with grain size calculated from XRD data due to clustering of strongly interacting grains in SEM images [34]. Nevertheless, both results confirmed the decrease of grain size with increasing milling time. SEM images of different samples revealed that grains of the bulk sample are adhesive to each other, while nano-sized grains form agglomeration in MH25 sample. The isolated nature of the grains in MH80 and MH300 samples indicated the reduction of inter-grain interactions for samples with higher milling time.

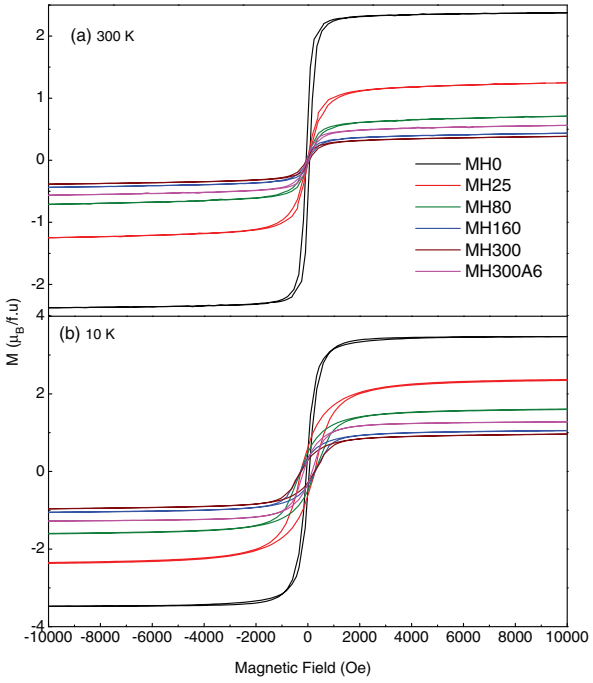

Fig. 3. Magnetic field dependence of magnetization at 300 K (a) and at 10 K (b) for bulk, milled and annealed samples. (For interpretation of the references to color in this figure legend, the reader is referred to the web version of the article.)

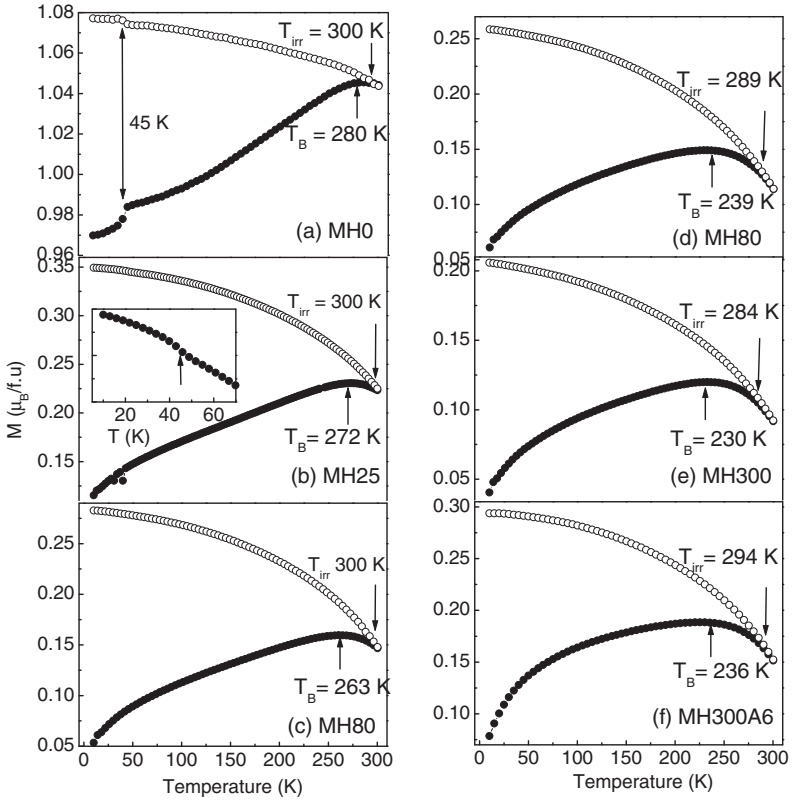

Fig. 4. (a–f) Temperature dependence of zero filed cooled (red symbol) and field cooled (black symbol) magnetization at 100 Oe for different samples. Magnetic irreversibility at T_{irr} and blocking at T_B are shown by arrows. Magnetic anomaly at 45 K is shown by dotted arrows.

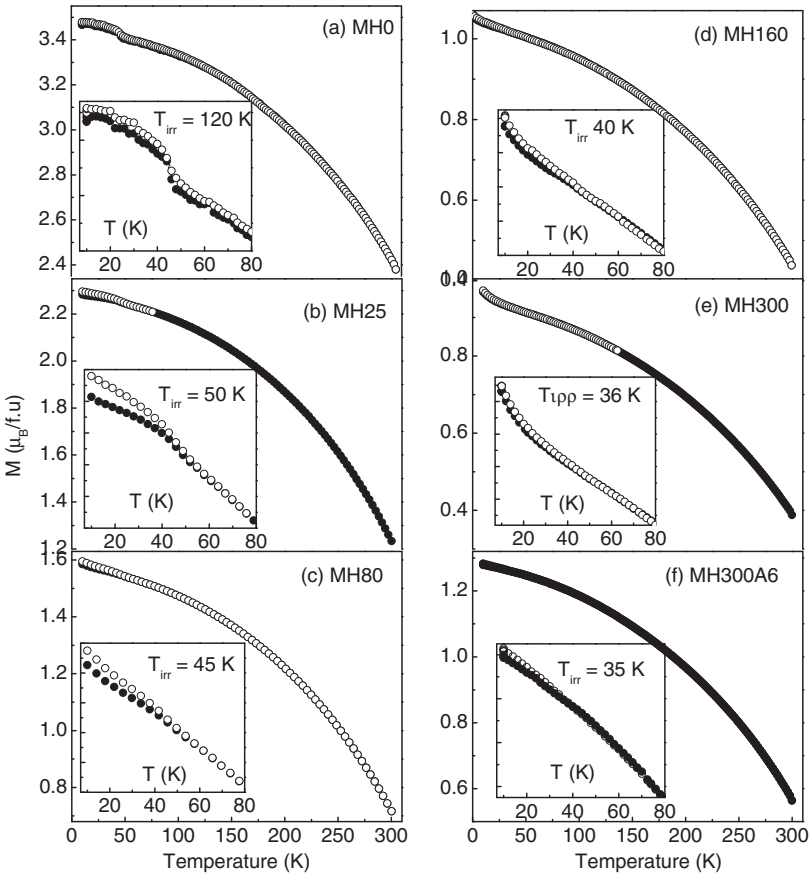

Fig. 5. (a–f) Temperature dependence of ZFC (red symbol) and FC (black symbol) magnetization at 10 kOe for different samples. Inset figures show the magnetic irreversibility and magnetic up turn at low temperatures.

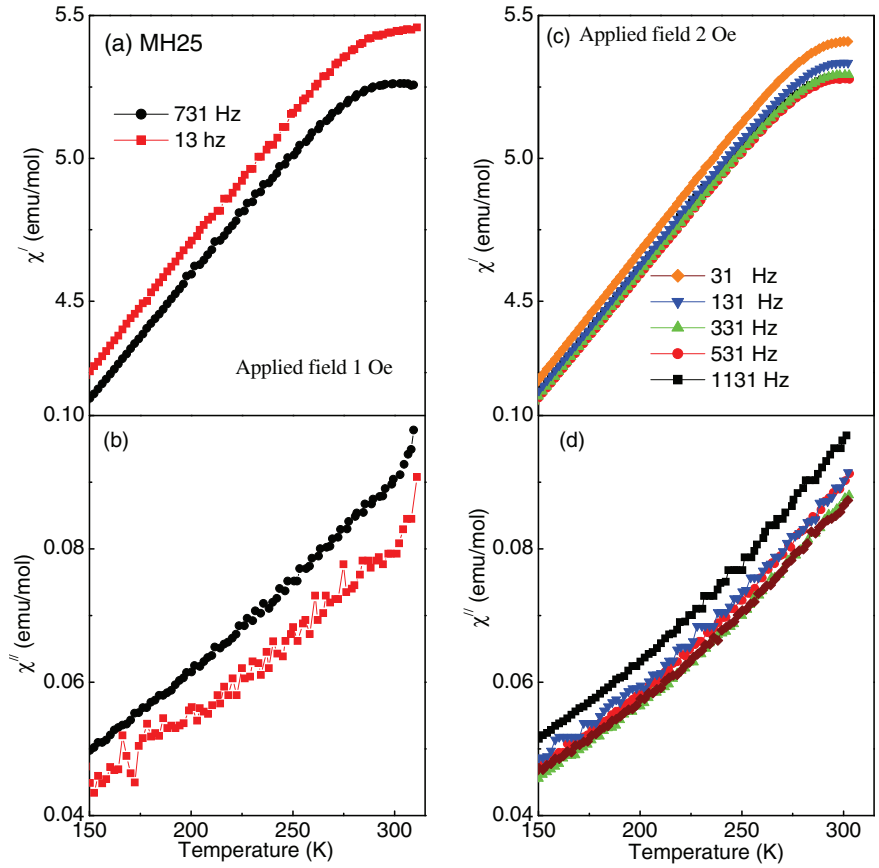

Fig. 6. Temperature dependence of $\chi^{/}$ (a and c) and $\chi^{//}$ (b and d) of ac susceptibility of MH25 sample at applied field 2 Oe and 1 Oe for selected applied frequencies of MH25 sample.

3.2. dc magnetization

Fig. 3 shows the magnetic field (H) dependent dc magnetization (M) at 300 K (Fig. 3(a)) and 10 K (Fig. 3(b)). The samples are typical soft ferromagnet with small loop at 300 K. Magnetization is nearly saturated above 1 kOe due to rotation of magnetic domains in bulk sample. A non-saturated $M(H)$ curve of milled samples above 1 kOe shows increasing spin disorder in ferromagnetic grains [3]. Non-saturated magnetic feature is also confirmed from the larger value of saturation magnetization (M_{Sat}: calculated from M vs. $1/H$ plot at $1/H \rightarrow 0$) than the spontaneous magnetization (M_S: calculated from linear extrapolation of high field (>5 kOe) $M(H)$ data at $H = 0$). Table 1 shows the important magnetic parameters using the $M(H)$ data. Finite ferromagnetic moment, i.e., M_S, at 300 K suggest that T_C of the bulk and milled samples is above room temperature. The low temperature (at 10 K) $M(H)$ curves at high fields (>4 kOe) are nearly identical to the 300 K features, except magnetization and hysteresis loop are substantially large at 10 K. The observed M_{Sat} of bulk sample (~3.49 μ_B/f.u. at 10 K) is close to the theoretical value 3.67 μ_B and experimentally reported value 3.59 μ_B measured at 5 K [38]. Ferromagnetic moment of bulk sample at 300 K (~2.4 μ_B/f.u.) reduces to ~0.5 μ_B/f.u. in MH300 sample due to increasing surface spin disorder. M_R/M_S (M_R is the remanent magnetization and defined as the retaintivity of magnetization after the magnetic field reduces to zero from ±50 kOe) ration (~0.15) of the bulk sample at 10 K improves to the maximum value ~0.37 for MH160 sample. Then, there is a small decrease of M_R/M_S (~0.31) for MH300 sample. Increase of ferromagnetic coercivity (H_C) with the decrease of grain size indicated a transformation from multi-domain state to single domain state of the ferromagnetic grains. The single domain magnetic state with improved M_R/M_S ration and $T_C > 300$ K are useful for developing soft ferromagnetic data storage materials. MH300 sample after annealing at 600 °C (MH300A6 sample) has achieved higher values of M_{Sat} and M_S. This shows that thermal activated grain size increase can restore the properties of bulk sample, which may not be identical to bulk sample due to different microstructure in annealed sample [32]. The magnetic moment and features of the MH300A6 sample is in between MH160 and MH80 samples.

Fig. 4 shows the zero field cooled magnetization (MZFC) and field cooled magnetization (MFC) curves of different samples at 100 Oe and temperature scale 300–10 K. Both bulk and nano-grained samples exhibited large separation between MZFC and MFC curves below magnetic irreversible temperature T_{irr}. Magnetic irreversibility shows some intrinsic spin disorder and frustration related to the domain freezing/pinning in the ferromagnetic ground state of the bulk sample of manganites [5,31,39]. These spin disorder is more in nano-grain size milled samples. Magnetic irreversible temperature T_{irr} for bulk, MH25 and MH80 samples is at ≥300 K, but definitely reduced below 300 K for MH160 and MH300 samples. MZFC shapes into a maximum at T_B ($<T_{irr}$), known as blocking temperature, and MZFC decreases below T_B due to blocking of ferromagnetic domains (clusters) [31,40,41]. However, MFC continuously increases below T_{irr} for all samples. We noted an abrupt magnetic jump at about 45 K for bulk sample, where MZFC rapidly decreased below 45 K and MFC has increased. Similar magnetic anomaly at 40–45 K observed in some of the nanoparticle manganites mainly in MFC curve [9,15]. In contrast, we find such abrupt increase of MFC in micron grain sized bulk sample and associated MZFC drop is drastically different from the reported features of nano-grained samples. Nanocrystalline milled samples, in our case, showed a shoulder type magnetic freezing below 45 K. The abrupt increase of MFC at 45 K is very weak for MH25 sample (inset of

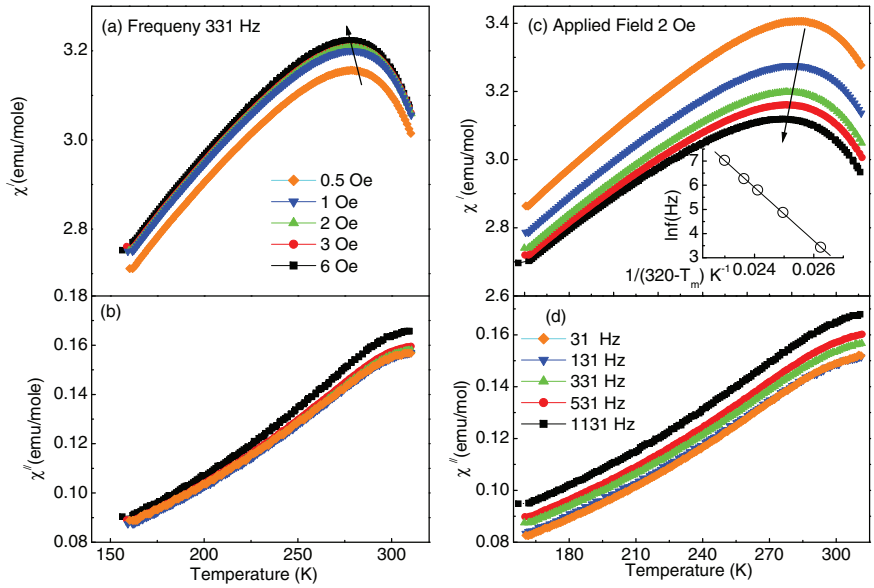

Fig. 7. Temperature dependence of real (χ') and imaginary (χ'') parts of ac susceptibility at 331 Hz for different field amplitudes (a and b) and at 2 Oe field amplitude for different frequencies (c and d) of MH300 sample, respectively. Inset of (c) shows the fit of peak temperature T_m with Eq. (1).

Fig. 4(b)) and gradually disappears on further decreasing the grain size by mechanically milling. Bhowmik et al. [31] identified similar magnetic anomaly in bulk $La_{0.67}Ca_{0.33}MnO_3$ and subsequent grain size effects through ac susceptibility study. We suggest that such low temperature anomaly is not strictly due to surface spin freezing effect, as ascribed in earlier reports [9,15]. If it is due to surface spin freezing alone, one could have expected stronger effect of low temperature magnetic anomaly for the nano-grained samples. However, it did not happen in mechanically milled samples. Moreover, increasing surface spin disorder decreased both T_{irr} and T_B in mechanically milled samples. The increase of grain size and annealing of grain boundary disorder in MH300A6 sample again increased both T_B and T_{irr}. MH300A6 sample also regained the shouldering effect in MZFC at 45 K (Fig. 4(f)).

Fig. 5 shows that 10 kOe field overcomes the freezing of ferromagnetic domains and magnetization continuously increases below 300 K, irrespective of MZFC and MFC curves. Insets of Fig. 5 show a drastic decrease of magnetic separation between MZFC and MFC, and confirmed the decrease of T_{irr} with grain size. It is a coincidence that temperature dependence of MZFC–MFC of mechanically milled MH80 sample (grain size ~10 nm) at 10 kOe is identical to the features of the same compound prepared by chemical route and measured at 50 kOe [9]. The low temperature magnetic upturn in Fig. 5(d and e), a typical reflection of surface spin disorder [42], in MZFC and MFC curves of MH160 and MH300 samples is different from the down curvature of larger grain-sized (bulk, MH25, and MH80) samples. The magnetic features of MH300A6 sample (Fig. 5(f)) lie in between MH160 and MH80 samples. The remarkable point is that magnetic jump of the bulk sample is also at 45 K for both MZFC and MFC curves at 10 kOe. This means magnetic anomaly at 45 K is magnetic field independent and we exclude its origin due to spin glass freezing. The observed magnetic anomaly may be attributed to the presence of small amount of parasitic phase Mn_3O_4 (magnetic ordering temperature ~43 K) beyond the detection limit from XRD pattern [43]. This Mn_3O_4 phase leads to the formation of short range ordered antiferromagnetic superexchange interactions between of Mn^{3+} ions. The coexistence of antiferromagnetic superexchange interactions and ferromagnetic double exchange interactions of Mn^{3+}/Mn^{4+} ions introduces inhomogeneous exchange interactions inside some of the clusters [43–45]. Such heterogeneity in intra-cluster interactions is dominated over by the surface disorder in nano-grain sized milled samples.

3.3. ac susceptibility

We have measured the temperature (75–310 K) dependence of ac susceptibility (real: χ' and imaginary: χ'') of the two end members (MH25 and MH300) for understanding the nature of magnetic blocking/freezing below T_B. The data in Figs. 6 and 7 are plotted in the temperature range 150–310 K for clarity. Fig. 6(a and b) and (c and d) show the ac susceptibility data of MH25 sample at selected frequencies for field amplitudes 1 Oe and 2 Oe, respectively. Fig. 7(a and b) and (c and d) shows the susceptibility data of MH300 sample at different field amplitudes and frequencies, respectively. It is clear that blocking temperature of MH25 sample is higher (at ≥300 K) than that for MH300 sample (at <300 K). Both χ' and χ'' are increasing with the increase of temperature in MH25 and MH300 samples. The $\chi''(T)$ peak seems to be at the inflection point of $\chi'(T)$ peak at temperature T_m. The unusual feature is that peaking of $\chi''(T)$ definitely occurs at $T > T_m$ in both samples, unlike the conventional $\chi''(T)$ peak at $T < T_m$ for traditional spin glass/superparamagnets [46]. Nanocrystaline $La_{0.67}Ca_{0.33}MnO_3$ samples [31] also showed similar $\chi''(T)$ peak at the inflection point of $\chi'(T)$ peak at $T > T_m$. Otherwise, the features of a monotonic decrease of χ' magnitude and increase of χ'' magnitude with increasing frequency are consistent with traditional spin glass or superparamagnet [46]. We have further examined the effects of varying field amplitudes and frequencies on MH300 sample considering its well defined $\chi'(T)$ peak at T_m ~280 K (within the measurement temperature range). $\chi'(T)$ peak in Fig. 7(a) has shown a small shift for increasing field amplitude from 0.5 Oe to 6 Oe at 331 Hz. The magnitude of $\chi'(T)$ (Fig. 7(a)) and $\chi''(T)$ (Fig. 7(b)) both have increased with the increase of field amplitude, showing field induced ordering of ferromagnetic domains or clusters. The remarkable feature is that χ' peak (Fig. 7(c)) shifted to lower temperature with the increase of applied frequency from 31 Hz to 1131 Hz. Similar frequency shift of the $\chi'(T)$ peak has been indicated in chemical routed $La_{0.67}Sr_{0.33}MnO_3$ nanoparticles [47], although authors have assumed higher temperature shift of the peak. Such observation is not consistent to the properties of traditional spin glass/superparamagnet [46,48]. In traditional

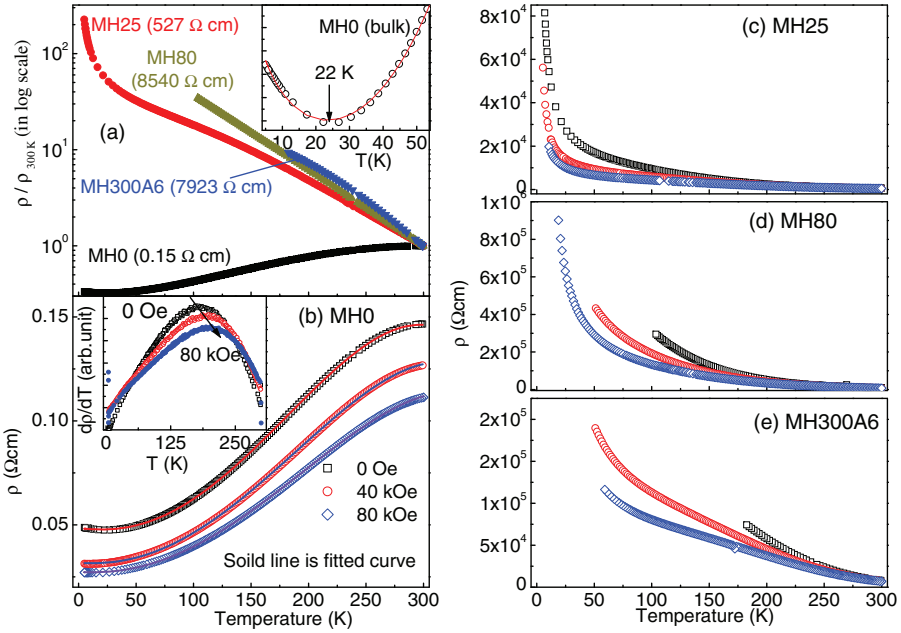

Fig. 8. Temperature dependent normalized resistivity curves $\rho(T)/\rho(300\,K)$ for selected samples (a). The resistivity at 300 K is shown against each sample. Inset of (a) shows the fitted data of resistivity minimum at 22 K for bulk sample. $\rho(T)$ curves at different magnetic field for selected samples (b–e). Inset of (b) shows the first order derivative of $\rho(T)$ curves ($d\rho(T)/dT$) for bulk samples. Arrow indicates the shift of the maximum of derivative curve with increasing field.

spin glass $\chi'(T)$ peak is expected to shift to higher temperature (T_m) by increasing frequency (f) according to Vogel–Fulcher law: $f = f_0 \exp[-E_a/k_B(T_m - T_0)]$ [46]. However, the observed peak shift is well fitted (inset of Fig. 7(c)) to the modified equation:

$$f = f_0 \exp\left[\frac{-E_a}{k_B(T_0 - T_m)}\right] \quad (1)$$

In our fit expression, the critical temperature T_0 (~320 K) amounting strength of inter-cluster interactions is higher than the freezing temperature T_m (~280 K) of the ferromagnetic clusters, unlike $T_0 < T_m$ for conventional spin glass freezing. The activation energy is ~95 meV and attempt frequency (f_0) is ~10^{14} Hz. As expected for long ranged ferromagnet, freezing of ferromagnetic domains started below T_C and T_0 is lying in between T_C (>300 K) and the average freezing temperature of the domains at T_m ~280 K. In the presence of additional spin disorder in milled samples in terms of the distribution of cluster size, intra-cluster exchange interactions, anisotropy energy and disorder at grain boundaries, the clusters may respond to ac magnetic field at different temperature scale depending on the driven frequency. We understand that ferromagnetic interactions among the magnetic domains (spin clusters) are sufficiently strong in the present nano-grained samples and intra-cluster structure, as well as interactions are playing a major role in this unusual freezing of clusters [16,49].

3.4. dc resistivity and magnetoresistance

We have measured dc resistivity (ρ) of the samples in the temperature (T) range 5–300 K. Viewing different order of $\rho(T)$ of the samples, Fig. 8(a) shows normalized temperature dependent resistivity of MH0, MH25 and MH80 samples. Table 2 shows the $\rho(300\,K)$ of the samples used for normalization. The low temperature (at 22 K) resistivity minimum of the bulk sample is absent in nano-grained samples. The $\rho(T)$ curve of nano-grained samples showed insulator/semiconductor type increase below 300 K and the increase is rapid at lower temperature. We understand that $\rho(T)$ minimum of the bulk sample appeared due to competition between weak ferromagnetic (semiconductor/insulator) grain boundaries and ferromagnetic (metallic) grains. Magnetic disorder and frustration in the ferromagnetic ground state of manganites [43–45] are affecting the low temperature resistivity upturn. Additional grain boundary disorder (spin canting, breaking of long ranged ferromagnetic order) is enough for the disappearance of resistivity minimum in nanocrystalline samples. Some of the nano-grained manganites,

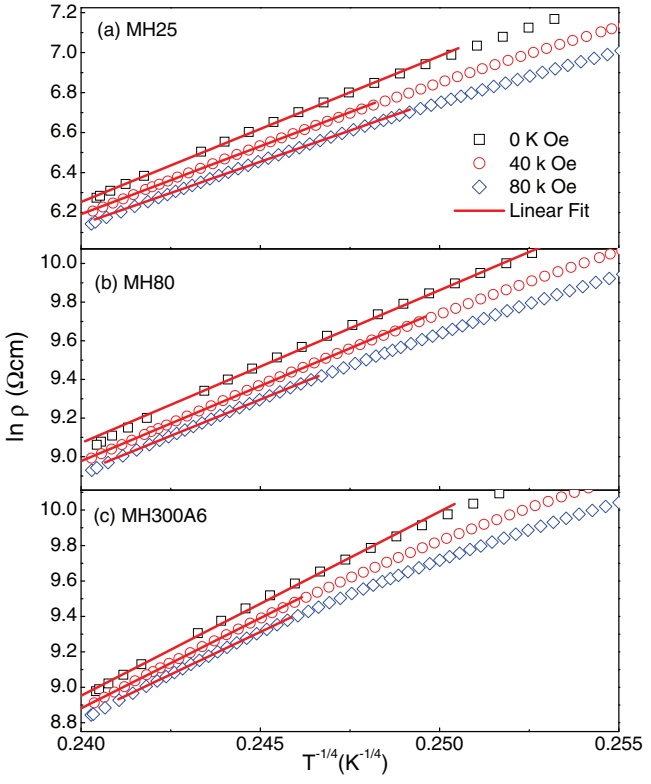

Fig. 9. (a–c) The fit of high temperature $\rho(T)$ curves to Eq. (3) of MH25, MH80 and MH300A6 samples, respectively.

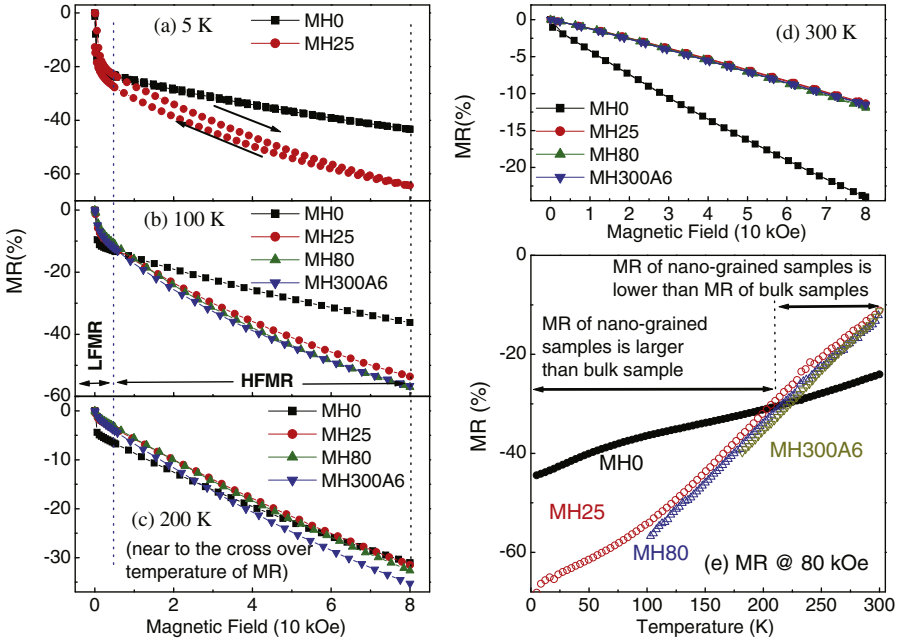

Fig. 10. MR(H) for bulk and selected nano-grained samples at 5 K (a), 100 K (b), 200 K (c), 300 K (d), and temperature dependence of MR(80 kOe) for selected samples (e). Note 200 K is near to the cross over temperature where MR of bulk and nano-grained samples are nearly same order.

irrespective of chemical route [15,27,28] or mechanically milling [34], exhibited low temperature resistivity maximum that we did not see in our samples. This shows that grain size effect alone does not control the low temperature resistivity shape; rather surface spin structure and surface morphology of nano-sized grains played important roles [32]. $\rho(T)$ data (inset of Fig. 8(a) shows the fit of resistivity minimum) in the whole temperature range of the bulk sample are well fitted with the equation:

$$\rho(T) = \rho_0 + \rho_{1/2}T^{1/2} + \rho_{3/2}T^{3/2} + \rho_4 T^4 \quad (2)$$

In Eq. (2) ρ_0 is the residual resistivity due to intrinsic disorder, $T^{1/2}$ term arises from low temperature electron–electron coulomb interactions, $T^{3/2}$ term arises due to electron–magnon interactions in the ferromagnetic metallic state and T^4 term arises due to electron–phonon interactions/spin fluctuation in ferromagnetic matrix. Fig. 8(b) shows a gradual disappearance of the $\rho(T)$ minimum of the bulk sample as an effect of increasing magnetic field, and high magnetic field, e.g., 80 kOe, suppressed the low temperature resistivity up turn. This is due to field-induced ordering of magnetic domains at grain boundaries [50] that results in an increasing metallicity in the ferromagnetic matrix [29]. Table 2 shows the fit parameters of Eq. (2). It is noted that all fit parameters (ρ_0, $\rho_{1/2}$, $\rho_{3/2}$ and ρ_4) gradually decreases as an effect of increasing magnetic field. The $\partial\rho(T,H)/\partial T$ vs. T plot (inset of Fig. 8 (b)) shows a peak near to the inflection point of the corresponding $\rho(T,H)$ curves. The shift of $\partial\rho(T,H)/\partial T$ peak to higher temperature by increasing H is an effect of high temperature shift of the colossal magnetoresistance (CMR) peak with increasing magnetic field. One can see that CMR peak of bulk sample is incomplete within the measurement temperature up to 300 K. Although applied field strongly affects the $\rho(T,H)$ curves of the nano-grained samples (Fig. 8(c–e)); none of them exhibited resistivity minimum for field up to 80 kOe. Otherwise, increase of field drastically reduces the low temperature rapid increase of $\rho(T)$. This suggests that milling introduced disorder at the surfaces/grain boundaries reduces metallic property of the ferromagnetic grains and surface/grain boundary spins are actively responding to the increasing field, resulting in the reduction of electrons scattering. We have found in Fig. 9(a–c) that Mott's 3D variable range hopping (VRH) model [51] with following equation fits the $\rho(T,H)$ curves of nano-grained samples:

$$\rho = \rho_0 \exp\left(\frac{T_0}{T}\right)^{1/4} \quad (3)$$

Here, $T_0 = [16\alpha^3/k_B N(E_F)$, ρ_0 is constant, k_B is Boltzmann constant and α describes the spatial extent of the localized wave function. The slope of the plots ln $\rho(T)$ vs. $1/T^{1/4}$ (Fig. 9) was used to estimate T_0 and density of states $N(E_F)$ at the Fermi level using $\alpha = 2.22\ \text{nm}^{-1}$ [52] for different nano-grained samples. The obtained values of $N(E_F)$ are shown in Table 2. $N(E_F)$ decreases with the decrease of grain size that results in the decrease of ferromagnetic spin polarization at the Fermi level and responsible for the increasing insulator/semiconductor character [5]. Magnetic field increased $N(E_F)$, but spin polarized ferromagnetic ground state of bulk samples is not recovered in milled samples.

Fig. 10 shows the field dependent magnetoresistance [MR(H) = ($\rho(H) - \rho(0)$)/$\rho(0)$] of the samples at 5 K (Fig. 10(a)), 100 K (Fig. 10(b)), 200 K (Fig. 10(c)) and 300 K(Fig. 10(d)). MR is negative for all samples. Fig. 10(a) shows that there is a sharp drop of MR(H) at 5 K below 5 kOe for both bulk and MH25 samples. Spin polarized tunneling of charge carriers between

Table 2
Electrical fit parameters using temperature dependence of resistivity curves [Eq. (2)] for sample MH0 and Variable Range Hopping model (VRH) [Eq. (3)] for milled samples.

Magnetic field (10 kOe)	MH0				$N(E_F) \times 10^{18}$ (eV^{-1} cm^{-3})		
	ρ_0 (Ω cm)	$\rho_{1/2}$ (10^{-6} Ω cm/K$^{1/2}$)	$\rho_{3/2}$ (10^{-5} Ω cm/K$^{3/2}$)	ρ_4 (10^{-11} Ω cm/K^4)	MH25	MH80	MH300A6
0	0.048	3.92	−2.01	−1.65	5.97	4.33	1.45
4	0.032	2.82	−1.90	−1.15	7.96	4.61	1.57
8	0.027	2.35	−1.00	−9.04	10.1	5.33	2.00

ferromagnetic grains contributes to this MR drop at low field regime, known as low field magnetoresistance (LFMR) [10]. The sharpness of decreasing MR(H) is small in MH25 sample. The high field (>5 kOe) magnetoresistance (HFMR) of MH25 sample is slowly decreasing in comparison with low field regime. Magnitude of HFMR of the bulk sample at 5 K is always smaller than the MH25 sample (smaller grains), because disordered grain boundary spins or magnetic spin clusters of the nano-sized grains mainly contributes to HFMR [14]. Response of these disordered spins to the magnetic field is slow due to interactions among spins and this provides a large scope of tuning HFMR [5]. Relaxation of these grain boundary spins exhibited hysteresis loop of HFMR at 5 K with magnetic field cycling in MH25 sample. Such loop is absent in bulk sample, because ferromagnetic order of the spins is already saturated at low field regime (Fig. 3) and small decrease of HFMR appeared due to coexisting magnetic clusters in the ferromagnetic matrix. As an effect of increasing measurement temperatures, magnitude of LFMR strongly decreases at 100 K and 200 K in all samples. At 300 K, bulk sample shows nearly 1% LFMR but there is no significant LFMR for milled samples. Magnitude of HFMR decreases at higher temperature and the decrease is faster for nano-grained samples. Consequently, there is a cross over from higher magnitude of HFMR for milled sample (~68% for MH25) than bulk sample (~45%) at 5 K to nearly same range of HFMR for milled and bulk samples at 200 K. Although HFMR of milled samples at 300 K (~12%) is smaller than the bulk sample (~30%), this value is still larger than the value (~4%) of many chemical routed samples [7]. The low temperature value (~60–65%) of our samples is comparable to reported work [53]. Temperature dependence of the magnetoresistance [MR(T) = (ρ(T, 80 kOe) − ρ(T, 0 kOe))/ρ(T, 0 kOe)] in Fig. 10(e) confirmed the cross over regime of MR at 200–230 K in nanocrystalline samples. The decrease of HFMR at higher temperature indicates the decrease of ferromagnetic double exchange correlation among the grain boundary Mn^{3+}–O^{2-}–Mn^{4+} spins networks and such effect is rapid in milled samples. According to core–shell spin structure of ferromagnetic grains [31,35], some of the grain boundary (shell) spins become paramagnetic or disordered with the decrease of grain size. Although T_C of bulk and milled samples is above 300 K, the fraction of paramagnetic spins at grain boundaries increases as the temperature increases to 300 K and less contributing to field induced change in HFMR.

4. Conclusions

Magnetic anomaly of bulk LSMO sample at 45 K is not due to surface spin freezing effect. We understand such anomaly in terms of heterogeneous exchange interactions inside some of the clusters existing in ferromagnetic matrix. Increasing surface disorder of mechanically milled samples dissolves such heterogeneity of intra-cluster interactions at the grain boundaries. Increasing spin disorder at grain boundaries has shown few more effects that are dramatic, e.g., crossing over of HFMR at about 200 K, loss of metallic conductivity, and unconventional freezing of ferromagnetic domains. The grain boundary disorder in the ferromagnetic matrix is enough for the loss of spin polarized tunneling of the charge carriers and subsequent decrease of LFMR in milled samples. The milled samples provide a large scope for tuning HFMR and their liner field dependent HFMR could be useful for magnetic sensor application.

Acknowledgments

We thank Dr. A. Banerjee and Dr. R. Rawat of UGC-DAE CSR, Indore, for providing magnetic and electrical measurement facilities. We thank CIF, Pondicherry University for SEM measurement. RNB thanks to UGC for research grant [F.NO. 33-5/2007(SR)]. IPM, thanks to CSIR for awarding SRF (09/559/(0060)/2010/EMR-I).

References

[1] V.F. Puntes, K.M. Krishnan, A.P. Alivisatos, Science 291 (2001) 2115.
[2] S. Dong, F. Gao, Z.Q. Wang, J.-M. Liu, Z.F. Ren, Appl. Phys. Lett. 90 (2007) 082508.
[3] W.J. Lu, X. Luo, C.Y. Hao, W.H. Song, Y.P. Sun, J. Appl. Phys. 104 (2008) 113908.
[4] S.L. Cheng, J.L. Lin, J. Appl. Phys. 98 (2005) 114318.
[5] D.D. Sarma, S. Ray, K. Tanaka, M. Kobayashi, A. Fujimori, P. Sanyal, H.R. Krishnamurthy, C. Dasgupta, Phys. Rev. Lett. 98 (2007) 157205.
[6] A. de Andres, M. Garcia-Hernandez, J.L. Martinez, C. Prieto, Appl. Phys. Lett. 74 (1999) 3884.
[7] P. Dey, T.K. Nath, Appl. Phys. Lett. 89 (2006) 163102.
[8] P. Dey, T.K. Nath, U. Kumar, P.K. Mukhopadhyay, J. Appl. Phys. 98 (2005) 014306.
[9] T. Zhu, B.G. Shen, J.R. Sun, H.W. Zhao, W.S. Zhan, Appl. Phys. Lett. 78 (2001) 3863.
[10] H.Y. Hwang, S.-W. Cheong, N.P. Ong, B. Batlogg, Phys. Rev. Lett. 77 (1996) 2041.
[11] C. Zener, Phys. Rev. 82 (1951) 403.
[12] A.J. Millis, P.B. Littlewood, B.I. Shraiman, Phys. Rev. Lett. 74 (1995) 5144.
[13] E. Dagotto, S. Yunoki, A.L. Malvezzi, A. Moreo, J. Hu, S. Capponi, D. Poilblanc, N. Furukawa, Phys. Rev. B 58 (1998) 6414.
[14] S. Lee, H.Y. Hwang, B.I. Shraiman, W.D. Ratcliff II, S.-W. Cheong, Phys. Rev. Lett. 82 (1999) 4508.
[15] P. Dey, T.K. Nath, P.K. Manna, S.M. Yusuf, J. Appl. Phys. 104 (2008) 103907.
[16] V. Markovich, I. Fita, A. Wisniewski, G. Jung, D. Mogilyansky, R. Puzniak, L. Titelman, G. Gorodetsky, Phys. Rev. B 81 (2010) 134440.
[17] V. Kusigerski, D. Markovic, V. Spasojevic, M. Tadic, M. Zentkova, M. Mihalik, J. Nanopart. Res. 12 (2010) 1299.
[18] Z. Jirák, E. Hadová, O. Kaman, K. Knížek, M. Maryško, E. Pollert, M. Dlouhá, S. Vratislav, Phys. Rev. B 81 (2010) 024403.
[19] Y. Wang, H.J. Fan, Appl. Phys. Lett. 98 (2011) 142502.
[20] M. Pekala, V. Drozd, J.F. Fagnard, Ph. Venderbemden, M. Ausloos, J. Appl. Phys. 105 (2009) 013923.
[21] X.J. Chen, H.U. Habermeier, H. Zhang, G. Gu, M. Varela, J. Santamaria, C.C. Almasan, Phys. Rev. B 72 (2005) 104403.
[22] E. Rozenberg, M. Auslender, I. Felner, G. Gorodetsky, J. Appl. Phys. 88 (2000) 2578.
[23] S. Mukhopadhyay, I. Das, J. Phys.: Condens. Matter 21 (2009) 186004.
[24] E. Rozenberg, J. Appl. Phys. 101 (2007) 036105.
[25] E. Rozenberg, J. Supercond. Nov. Magn. 23 (2010) 183.
[26] Z. Chen, Y. Xu, Y. Su, S. Cao, J. Zhang, J. Supercond. Nov. Magn. 22 (2009) 465.
[27] D.K. Pandya, S.C. Kashyap, G.R. Pattanaik, J. Alloys Compd. 326 (2001) 255.
[28] A. Dutta, N. Gayathri, R. Ranganathan, Phys. Rev. B 68 (2003) 054432.
[29] S. Kundu, T.K. Nath, J. Phys.: Condens. Matter 22 (2010) 506002.
[30] P. Dey, T.K. Nath, Phys. Rev. B 73 (2006) 214425.
[31] R.N. Bhowmik, A. Poddar, R. Ranganathan, C. Mazumdar, J. Appl. Phys. 105 (2009) 113909.
[32] R.N. Bhowmik, R. Ranganathan, R. Nagarajan, B. Ghosh, S. Kumar, Phys. Rev. B 72 (2005) 094405.
[33] P. Kameli, H. Salamati, A. Aezami, J. Appl. Phys. 100 (2006) 053914.
[34] I. Panagiotopoulos, N. Moutis, M. Ziese, A. Bollero, J. Magn. Magn. Mater. 299 (2006) 94.
[35] R.N. Bhowmik, J. Magn. Magn. Mater. 323 (2011) 311.
[36] A. Bajpai, A. Banerjee, Rev. Sci. Instrum. 68 (1997) 4075.
[37] I.P. Muthuselvam, R.N. Bhowmik, J. Magn. Magn. Mater. 322 (2010) 767.
[38] G.J. Snyder, R. Hiskes, S. DiCarolis, M.R. Beasley, T.H. Geballe, Phys. Rev. B 53 (1996) 14434.
[39] A. Poddar, R.N. Bhowmik, I.P. Muthuselvam, N. Das, J. Appl. Phys. 106 (2009) 073908.
[40] S.M. Yusuf, M. Sahana, K. Dörr, U.K. Rößler, K.-H. Müller, Phys. Rev. B 66 (2002) 064414.
[41] J.W. Lynn, D.N. Argyriou, Y. Ren, Y. Chen, Y.M. Mukovskii, D.A. Shulyatev, Phys. Rev. B 76 (2007) 014437.
[42] R.N. Bhowmik, R. Nagarajan, R. Ranganathan, Phys. Rev. B 69 (2004) 054430.
[43] G. Dezanneau, M. Audier, H. Vincent, C. Meneghini, E. Djurado, Phys. Rev. B 69 (2004) 014412.
[44] P.K. Muduli, S.K. Bose, R.C. Budhani, J. Phys.: Condens. Matter 19 (2007) 226204.
[45] S.S. Pillai, G. Rangarajan, N.P. Raju, A.J. Epstein, P.N. Santhosh, J. Phys.: Condens. Matter 19 (2007) 496221.
[46] J.A. Mydosh, Spin Glasses, Taylor & Francis, London, 1993.
[47] A. Rostamnejadi, H. Salamati, P. Kameli, H. Ahmadvand, J. Magn. Magn. Mater. 321 (2009) 3126.
[48] I. Fita, V. Markovich, A. Wisniewski, D. Mogilyansky, R. Puzniak, P. Iwanowski, L. Meshi, L. Titelman, V.N. Varyukhin, G. Gorodetsky, J. Appl. Phys. 108 (2010) 063907.
[49] F. Rivadulla, M.A. Loïpez-Quintela, J. Rivas, Phys. Rev. Lett. 93 (2004) 167206.
[50] Y. Xu, J. Zhang, G. Cao, C. Jing, S. Cao, Phys. Rev. B 73 (2006) 224410.
[51] N.F. Mott (Ed.), Metal–Insulator Transition, vol. 67, 2nd ed., Taylor and Francis, London, 1991.
[52] A. Banerjee, S. Bhattacharya, S. Mollah, H. Sakata, H.D. Yang, B.K. Chaudhuri, Phys. Rev. B 68 (2003) 186401.
[53] Z. Zhang, R. Ranjith, B.T. Xie, L. You, L.M. Wong, S.J. Wang, J.L. Wang, W. Prellier, Y.G. Zhao, T. Wu, Appl. Phys. Lett. 96 (2010) 222501.